Molecular heterogeneity and differential metabolic signatures in thymic adipocytes

Joon Schwakopf,[1,2,3], Amber R. Syage,[1,3], Anca Franzini,[3,4], Katherine E. Varley,[3,4], Dean Tantin,[1,4]

[1]Department of Pathology, University of Utah School of Medicine, Salt Lake City, UT, USA.
[2]Department of Neurobiology, University of Utah School of Medicine, Salt Lake City, UT, USA.
[3]Huntsman Cancer Institute, University of Utah School of Medicine, Salt Lake City, UT, USA.
[4]Department of Oncological Sciences, University of Utah School of Medicine, Salt Lake City, UT, USA.

Correspondence: dean.tantin@path.utah.edu

Short title: Molecular characterization of thymic adipocytes

Keywords Thymus; T cells; Thymic epithelial cells; adipocytes; aging

Conflicts of interest statement: The authors have declared that no conflict of interest exists

Words in abstract: 180
Words main text: 5,610
Total main display items: 6

SUMMARY

Adipocyte depots throughout the body are physiologically and molecularly distinct. With age, adipocytes increase in and around aged thymi. However, thymic adipocytes completely lack molecular characterization. We developed and optimized methods to isolate adipocyte nuclei from mouse thymi of different ages and sexes. Single-nucleus multiomic analysis of male and female mice aged 4-9 months reveals that thymic adipocytes are heterogeneous, with at least two distinct populations. One subpopulation harbors a transcription and chromatin signature consistent with beige/brown fat. A larger subpopulation more strongly resembles classic white adipose tissue and expresses genes associated with epithelial-to-mesenchymal transition (EMT) and antigen presentation. Analysis of differentially open chromatin in the white compared to beige adipose population identifies binding sites for Foxn1 and HIF-1α/Arnt, consistent with a situation in which thymic white adipose cells emerge from thymic epithelial cells, possibly under hypoxic conditions. Immunofluorescence microscopy confirmed the expression of UCP1 protein in cells within the thymic parenchyma, most prominently in subcapsular cortical regions. This resource reveals a complex milieu of thymic adipocytes and identify multiple avenues for directly probing their ontogeny, dynamics and functional significance.

KEYWORDS

Thymus; Adipocytes; Beige Fat; PPARα; UCP1

INTRODUCTION

The thymus is the primary site of T cell development and education and thus plays a central role in adaptive immunity and central tolerance [1]. It consists of developing T cells (thymocytes), thymic epithelial cells (TECs), fibroblastic stromal cells and other less abundant cell types. The aging thymus also accumulates abundant and dynamic population of adipocytes [1], which we here term ThyAds.

With age, areas of the thymus devoted to thymopoiesis atrophy and T cell output declines in a process termed thymic involution [2]. Involution is associated with progressive disruption of the cortico-medullary junction, loss of thymic output, and increased adiposity in a manner influenced by biological sex and diet [3]. Attenuation of thymic output contributes to reduced TCR diversity, impaired pathogen response and increased susceptibility to infection [1,4-7]. Additionally, involution can be accelerated by administration of thiazolidinediones, implicating adipocyte expansion in this process [8], however their function in this process is unclear. Thymic involution is conserved across vertebrates and recapitulated in laboratory mice. Although severe infection, radiation, malnutrition, or hormonal alterations can induce acute thymic atrophy, age-related involution is the setting in which adipocyte accumulation is most consistently observed [1,3,9-11]. Despite their increasing abundance in the aging thymus, and the possibility that they have specialized functions analogous to other tissue-specific fat depots [12], ThyAds have yet been directly studied at the molecular level. Prior studies focused on thymocytes and thymic stromal cells have omitted ThyAds because intact adipocytes are large, buoyant, and fragile, and are therefore poorly captured by droplet-based microfluidic workflow [13-16].

Recent single-nuclei methodologies combining RNA-seq and ATAC-seq have enabled high-resolution mapping of adipose depots, including age-associated pro-inflammatory and metabolic shifts linked to obesity and related pathologies. These technologies have also shown that adipose depots are tailored to their local environment and differ in cellular and molecular composition across the body [12], and that adipocytes remodel over time [17,18]. In humans highly metabolically active brown adipose tissue (BAT), subcutaneous white adipose tissue (WAT), and beige fat, an intermediate form, typically decline with age wheras visceral WAT expands [19-21]. Together, these findings led us to hypothesize that ThyAds are distinct from other adipocyte populations and that their age-associated expansion reflects changes in cellular composition and state.

Here, we used an integrated multiomic strategy to generate the first single-nuclei dataset of ThyAds. By profiling nuclei rather than intact cells, multiomic sequencing overcomes the technical limitations imposed by adipocyte size and fragility. We develop methodologies to

efficiently liberate and isolate ThyAds and their nuclei from mouse thymi. By single-nucleus profiling, we identify two highly distinct ThyAd populations, termed ThyAd I and ThyAd II. ThyAd I exhibit a beige fat-like transcriptional program, whereas ThyAd II show features consistent with classic WAT. Notably, ThyAd II-specific accessible chromatin was enriched for consensus sites recognized by Foxn1, the master transcription regulator of TECs. This enrichment suggests a TEC-linked regulatory signature and supports the hypothesis that ThyAd II derive from TECs. Together, our ThyAd multiome resolves two adipocyte programs and provide clues to cellular origin, providing a roadmap to test lineage relationships and functional roles in thymic aging.

RESULTS

ThyAds comprise two discrete subpopulations, one of which has transcriptional hallmarks of beige fat

Thymic adipocytes are technically difficult to recover. We successfully developed an enrichment workflow that combines a retina tissue dissociation protocol and WAT buoyancy-based fractionation, followed by single-nuclei isolation to profile 6-month-old female mice (**Figure 1A**). In mature thymi, scattered multilocular lipid-laden cells are detectable within the subcapsular region, parenchyma, and PVS by ~3 months, while large unilocular white adipocytes become prominent after ~12 months [22]. We therefore reasoned that 6-month-old mice would capture maximal diversity in the ThyAd pool, at a timepoint when thymic output is still preserved but ThyAds are recoverable from a sufficient amount of thymic tissue. After dissection, we extensively cleaned the thymic capsule to minimize contamination while preserving subcapsular and septal ThyAds (**Figure 1B**). Thymi were mechanically and enzymatically digested to generate a single-cell suspension, then fractionated to collect the buoyant adipocyte-enriched layer. Nuclei prepared from the buoyant fraction were robust, with preserved euchromatic and heterochromatic regions and nucleoli (**Figure S1A**).

16 pooled female thymi were used for single-nucleus ATAC-seq plus RNA-seq, yielding 3,610 high-quality nuclei after filtering (**Figure S1B**). Initial uniform manifold approximation and projection (UMAP) clustering indicated substantial hematopoietic carryover, with most nuclei expressing *Ptprc* (*Cd45*) and resolving into expected thymocyte populations based on canonical markers such as *Cd8a*, *Cd4*, *Mki67*, *Hes1* and *Cd5* (**Figure S1C,D**). For example, cluster 8 expressed *Il2ra* but not *Cd8a* or *Cd4*, identifying these cells as DN2/3. Cluster 2 expressed *Cd5* and likely comprised B cells. Cluster 7 expressed *Klrb1c*, which encodes the NK1.1 surface protein. These nuclei are likely derived from iNKT cells. In contrast, signatures of non-hematopoietic thymic stromal populations (TECs, fibroblasts/mesenchyme, endothelium) were minimal or absent. This may reflect either or both a greater abundance of bone marrow-derived cells in the thymus, or a closer apposition of these cells with ThyAds such that they are preferentially carried over with the buoyant fraction following digestion. These data establish a technical framework for ThyAd recovery and set the stage for targeted analysis of the ThyAd compartment.

Two transcriptionally discrete clusters (3 and 10) expressed the canonical adipocyte markers *Pparg* and *Plin1* (**Figure S1C**) as well as *Fabp4* (not shown), consistent with adipocytes. A lipid metabolism gene module further supported adipocyte identity in clusters 3 and 10, whereas cluster 11 (the least abundant cluster) showed weaker and less consistent expression of

122 adipocyte-associated transcripts (**Figure S2A**). We therefore focused on adipocyte clusers 3 and
123 10, yielding 429 high-quality adipocyte nuclei. These nuclei contained a mean of 1533 detected
124 genes and an average depth of 2974 reads per nucleus.

125 We re-clustered adipocyte based on gene expression (RNA-seq UMAP), chromatin
126 accessibility (ATAC-seq UMAP), and a weighted nearest neighbor (WNN) approach that
127 integrates both modalities (**Figure 1C**). This analysis resolved two broad transcriptional programs,
128 termed ThyAd I and ThyAd II, distinguished by differential expression of lipid metabolic genes
129 (**Figure S2B**). A small residual thymocyte cluster expressed *Themis* and *Satb1* (**Figure S3A**) as
130 well as lipid metabolic genes such as *Fasn* (**Figure S2B**) and may reflect doublet nuclei. The
131 remaining clusters lacked thymocyte gene expression and robustly expressed adipocyte markers
132 (e.g., *Pparg*), supporting their adipocyte identity (**Figures S2B** and **S3A**).

133 To define transcriptional states within ThyAds, we identified the top 10 DEGs across
134 clusters. This revealed clear separation between ThyAd transcription programs, with ThyAd I
135 more strongly expressing genes associated with thermogenesis relative to ThyAd II (**Figure S3A**).
136 Restricting analysis to adipocyte nuclei only, we further resolved five distinct ThyAD subclusters–
137 Ia, Ib, IIa, IIb and IIc (**Figure 1D**), consistent with prior evidence showing that ThyAds are
138 morphologically heterogeneous [22].

139 ThyAd Ia nuclei were marked by the expression of Prkar2b and *Fgf14*. In contrast, ThyAd
140 Ib more robustly expressed *Esrrg*, *Ucp1*, and *Cidea* (**Figure 1D**). *Ppara* was also up-regulated in
141 ThyAd Ib (**Table S1**). These genes have been shown to positively regulate beige adipocytes [23-25].
142 These findings strongly suggest that ThyAd I – particularly ThyAd Ib – are beige-like, consistent
143 with work that used imaging to identify UCP1-positive cells detected inside the thymic
144 parenchyma [22]. In contrast, ThyAd II nuclei expressed a distinct program consistent with WAT-
145 like identity (e.g., *Apoe*, **Table S1**) and additional features no observed in ThyAd I. ThyAd IIa was
146 enriched for epithelial-mesenchymal transition (EMT)-associated transcripts including *Prr16* and
147 *Alcam*, while ThyAd IIb/IIc displayed higher levels of *B2m* and *H2-D1* (**Figure 1D**), consistent with
148 increased MHC-I-related gene expression [26]. ThyAd II also expressed *Gpx3*, which has been
149 reported in thymic stromal populations including intermediary fibroblast-like states [27]. Additional
150 feature plots are shown in **Figure S3B**. These results indicate that ThyAd I (in particular ThyAd
151 Ib) resembles beige-like adipocytes, whereas ThyAd II is more WAT-like and exhibits an EMT-
152 /antigen-presentation-associated transcriptional signature.

153 Because ThyAd I and ThyAd II subclusters were readily distinguishable by the
154 thermogenic transcription signature in ThyAd I (**Figure 1D**), we combined the ThyAd Ia+Ib and
155 IIa+IIb+IIc subclusters, and performed differential expression analysis (**Table S2**). Gene

156 expression differences between combined ThyAd I and ThyAd II nuclei are shown in **Figure 2A**.
157 For example, *Prdm16* and *Ppara* were significantly enriched in ThyAd I, encoding transcriptional
158 regulators of beige/brown fat [28,29], while Retn and Prr16 were significantly enriched in ThyAd II,
159 encoding WAT-associated protein Prr16 [30] and the adipokine resistin, a regulator of adipogenesis
160 [31], respectively. Gene ontogeny (GO) analysis further supported functional divergence: ThyAd I
161 was enriched for pathways including "Mitochondrial organization" and "Positive regulation of cold-
162 induced thermogenesis", whereas ThyAd II was enriched for "Epithelial mesenchymal transition"
163 (**Figure 2B**).
164
165 **Single-nucleus ATAC-seq identifies state-specific chromatin accessibility and**
166 **transcriptional factor motif enrichment in ThyAds**
167 In addition to improving resolution of ThyAd states, the ATAC-seq component of the multiomic
168 dataset enables inference of regulatory programs by identifying transcriptional factor (TF) motifs
169 enriched in accessible chromatin. Moreover, because the chromatin state can precede or linger
170 relative to active gene expression, the chromatin states can reflect transcription potential as well
171 as recent enhancer decommissioning, providing information on the possible antecedents for given
172 populations. Because genomic DNA is fully preserved within the nuclei while much of the mRNA
173 is lost, the ATAC-seq portion of the data provides high-quality information on gene expression
174 states in isolated nuclei. We analyzed the ATAC-seq data focusing on genes associated with
175 beige adipocytes: *Ppara*, *Cidea* and *Ucp1*. In all cases, increased chromatin accessibility was
176 highly associated with the ThyAd Ib subcluster (**Figure 3A**). Additional genes are shown as
177 expression and ATAC accessibility feature plots in **Figure S4**.
178 To identify candidate TFs underlying ThyAd state differences, we compared TF motifs
179 enriched in between ThyAd I and ThyAd II. ThyAd I accessible regions were enriched for motifs
180 consistent with adipocyte differentiation and beiging, including EBF, Plagl1, PPAR and Esrrg
181 (**Figure 3B**). In contrast, ThyAd II accessible chromatin was enriched for Foxn1, hypoxia-inducible
182 factor-1 (HIF-1), Wilms tumor protein 1 (WT1), Krüppel-like factor 12 (KLF12), and KLF1 motifs.
183 Notably, Foxn1 is a master transcriptional regulator of thymic epithelial cells [32], suggesting a TEC-
184 linked regulatory imprint in the ThyAd II population. Together with the EMT signature associated
185 with ThyAd II gene expression (**Figure 1D and Figure 2B**), these results are consistent with a
186 model in which ThyAd II white adipose cells arise from TECs. Consistent with this interpretation,
187 transcripts encoding *Ebf2*, *Esrrg* and *Plagl1* were detected in subsets of ThyAD nuclei (**Figure**
188 **S4A**). In contrast, other TFs highlighted by motif enticement (including *Foxn1*) were not detectably
189 expressed, yet displayed accessible regulatory regions (**Figure S4A-B**, **Supplemental Tables**

190 **S1 and S2**), consistent with residual chromatin accessibility following recent TF activity or
191 enhancer decommissioning. Together, the data show increased accessibility at thermogenic loci
192 and enrichment of EBF, PPAR, and ESRRG motifs in ThyAd I, while ThyAd II is enriched for
193 FOXO1, HIF, and KLF1 motifs, consistent with a distinct and possibly TEC-linked regulatory
194 imprint.
195
196 **Younger (4-month-old) male mice harbor ThyAd I and II populations distinct from gonadal**
197 **fat**
198 We also profiled ThyAds from 4-month-old male mice to align sampling with the earlier kinetics of
199 thymic involution in males compared with females [33-35]. Whereas 6-month-old females provided
200 an optional window to capture ThyAd heterogeneity while thymic output remains relatively
201 preserved, we reasoned that males would reach a comparable stage of remodeling at an earlier
202 age. In mice, the thymus reaches near-maximal size around 5 weeks of age and then declines in
203 cellularity. In male C57BL/6 mice, thymic cellularity decreases by approximately 50% by 4 months
204 [36]. This is matched in human thymic tissue 26-49 years old, where the perivascular space (PVS)
205 comprises 50-60% of the thymic compartment and adipose tissue is easily identified [37]. We
206 therefore selected 4 months in males as a practical and biological window to capture ThyAds
207 during an early-to-intermediate phase of involution.
208 We isolated ThyAd nuclei from 6 male mice maintained on standard chow and profiled
209 them by single-nucleus RNAseq. From the same animals, we also collected gonadal (epididymal)
210 white adipose tissue (gWAT) as a visceral fat comparator (**Figure 4A**). As in the female dataset,
211 *Ptprc*+ nuclei carried through purification were manually removed prior to clustering. Joint
212 clustering of ThyAd and gWAT nuclei revealed that the thymic and gonadal adipocyte
213 transcriptomes were largely distinct, with ThyAd nuclei again segregating into two discrete
214 clusters (**Figure 4B**). A rare thymic cluster expressed *Esrrg*, *Ppara* and *Ppargc1b*, consistent with
215 a ThyAd I (beige-like) program (**Figure S5A**). In contrast, the ThyAd II cluster more closely aligned
216 with one of the gWAT clusters, suggesting a more WAT-like transcriptional state (**Figure 4B** and
217 **Figure S5A**). Feature plots confirmed strong expression of *Ppara* and *Esrrg* in ThyAd I (**Figure**
218 **4B-C**). These nuclei were also enriched for *Cidea* and *Ghr* (**Figure S5B**). When clustering thymic
219 nuclei alone, ThyAd I and II remained clearly separable, marked for example by *Ppara* and *Ghr*
220 (growth hormone receptor, **Figure 4D**). The most differentially expressed ThyAd I gene was
221 *Ppara*, whereas ThyAd II was enriched for *Xdh*, *Fabp4*, *Adgrl4*, *Klf12* and *Tgfb2* (**Table S3**).
222 Notably, *Tgfb2* (TGFβ2) has been implicated in promoting thymic [38]. Both populations expressed
223 core adipocyte genes including *Pparg* (**Figure 4D**) and *Cd36* (not shown).

224

225 **UCP1$^+$ cells largely localize within the subcapsular cortical thymic compartment, whereas**
226 **lipid-rich unilocular adipocytes localize to septa and perivascular space**

227 Epicardial/perithymic fat is heterogenous, with some beige-like cells strongly expressing UCP1
228 [39]. Although thymi used for sequencing were obtained from mice younger than 6 months old and
229 were extensively cleaned of extrathymic fat prior to processing (**Figure 1B**), it remained formally
230 possible that the beige-like ThyAd I signal reflected residual contamination outside the capsule.
231 Prior work, however, has identified UCP1$^+$ cells within the thymic parenchyma [22]. To directly
232 access localization, we performed Immunofluorescence on 6-month-old female thymi. For this
233 experiment, thymi were interntionally not cleaned of extrathymic fat, enabling direct comparison
234 of perithymic adipose tissue with intrathymic UCP1$^+$ cells.

235 As expected [39], perithymic fat and connective tissue abutting the thymic capsule was
236 heterogenous, with regions containing large unilocular lipid droplets and others containing
237 densely packed multilocular, BAT-like adipocytes with strong UCP1 staining. In contrast, UCP1$^+$
238 cells within the thymic parenchyma were sparse and exhibited weaker, punctate UCP1. Omission
239 of the primary antibody eliminated both the intra- and extrathymic UCP1 signal (**Figure 5**). In
240 parallel, PPARg staining and BODIPY labeling highlighted adipocytes with large unilocular lipid
241 droplets enriched within thymic septa and the perivascular space, consistent with ThyAd II (**Figure**
242 **S6**). Together, these data support the presence of beige-like ThyAd I cells within the thymic
243 capsule and argue against perithymic contamination as the primary source of the ThyAd I
244 transcriptional program detected by multiomic sequencing.

245 **DISCUSSION**

246 The thymus is a complex organ that facilitates the development and selection of thymocytes,
247 playing an important role in the maintenance of adaptive immunity and central tolerance. Cell
248 types associated with the thymus include thymocytes, TECs, fibroblastic/mesenchymal cells,
249 macrophages, DCs, B cells (particularly in the medulla), mature nonconventional T cells (e.g.,
250 iNKTs), endothelial cells, pericytes and nerves. During normal aging, thymic output declines via
251 a process termed thymic involution, contributing to established characteristics of age-related
252 immune senescence, such as reduced naive T-cell production and TCR diversity, chronic
253 systemic inflammation, and impaired pathogen response [1,37,40]. Involution is associated with
254 disruption of the cortico-medullary junction and increased adiposity [3].

255 Recent advances in single-nuclei methodologies combining RNA-seq and ATAC-seq have
256 been used to investigate the heterogeneity of adipose tissue depots throughout the body [12,41].
257 Separately, they have been used to profile thymocytes and thymic stromal cells [13-16]. However,
258 adipocytes associated with the thymus (ThyAds) remain uncharacterized at a molecular level.
259 Here, we developed methodologies to liberate and isolate adipocyte and their nuclei from mouse
260 thymi. We used an integrated multiomic sequencing strategy to generate the first single-nuclei
261 datasets of ThyAds and identify similarities and differences in transcriptional profiles compared to
262 a peripheral adipose depot. We profiled nuclei from female and male thymi at two different ages,
263 providing the first single-nucleus ThyAd atlas and expanding our understanding of ThyAds and
264 their potential roles in the thymus and during thymic involution. By single-nucleus profiling, we
265 identified two distinct ThyAd populations, termed ThyAd I and ThyAd II.

266 Adipocytes can be identified by their robust uptake and storage of triglycerides as neutral
267 lipid, as well as by release of fatty acids, with the balance regulated by metabolic demand. The
268 cellular and molecular composition of adipose tissue varies throughout the body in a manner
269 adapted to the tissue in which they are embedded [12]. For example, subcutaneous and visceral
270 WAT have distinct developmental origins, mechanisms of expansion and disease associations [42].
271 Adipocytes in different tissues closely interface with immune cells such as macrophages, DCs
272 and iNKTs, again in a manner tailored to the local environment, and can both suppress and
273 exacerbate inflammation depending on context [17,18,43,44]. We hypothesized that ThyAds are
274 qualitatively different from adipocytes in other fat depots, just as adipocytes in these depots are
275 different from one another.

276 snRNAseq revealed that ThyAds express mature adipocyte-associated markers such as
277 *Pparg*, *Fabp4*, and *Plin1*. No thymic preadipocytes were identified based on co-expression of

278 markers such as *Pdgfra/b*, *Pref1* and *Cd34* [45]. This is likely due to their relative lack of buoyancy.
279 These studies also revealed a population of ThyAds expressing a highly metabolically active
280 transcription program similar to beige adipose cells, termed 'ThyAd Ib'. These nuclei were
281 differentiated by significant expression of *Ucp1*, *Ppara* and *Esrrg*. , hallmarks of beige and brown
282 adipocytes. *Esrrg* for example encodes an orphan nuclear receptor expressed in metabolically
283 active tissues (e.g., brain, heart, skeletal muscle, BAT) that promotes adipocyte beiging by
284 activating mitochondrial biogenesis and oxidative metabolism [24]. *Ppara* encodes a nuclear
285 receptor associated with metabolically active tissues such as heart and brown adipose tissue
286 (BAT) that oxidize fatty acids at a high rate [46]. *Ppara* is also expressed in hepatocytes, where it
287 promotes fatty acid oxidation and ketogenesis during fasting [47,48]. In combination with PPARγ,
288 PPARα can induce beiging of white adipose tissue [49]. *Cidea*, which can be induced by the
289 combined expression of PPARγ and PPARα and encodes a transcription coregulator that
290 activates *Ucp1* expression [25]. *Prdm16* and *Ucp1* expression are also hallmarks of BAT [28].
291 PRDM16 represses type-1 interferon signaling in adipocytes which promotes thermogenic
292 programming [50].
293 Interestingly however, these nuclei did not strongly express other genes associated with beige
294 adipocyte gene expression programs, e.g. *Tbx1*, *Shox2*, *Tmem26*, or *Hoxc9*, indicating that
295 ThyAd Ib may be distinct from previously defined populations of beige adipocytes. An intermediate
296 population – 'ThyAd Ia' – shared expression of beige/brown genes with ThyAd Ib such as *Ppara*
297 and *Prdm16* but with little expression of *Ucp1*. DEG analysis of ThyAd clusters alone identified
298 *Acsl1*, *Prkr2b* and *Mecom* among the topmost ThyAd Ia-enriched genes. The products of these
299 genes are known to positively regulate adipogenesis and FA metabolism within BAT [51-53]. ThyAd
300 IIs displayed differential expression of genes such as *Col15a1*, *Prr16*, and *Pbx1*. These genes
301 are often associated with EMT and ECM remodeling [54-57]. EMT has been associated with more
302 plastic and stem-like states, allowing de-differentiation and developmental plasticity, including the
303 ability to transition to adipocytes [58]. Within the thymus, age-associated TECs (aaTECs) are also
304 associated with limited EMT signatures [27].
305 Analysis of transcription factor motifs enriched in open ThyAd chromatin supports the
306 finding of two broad transcriptional ThyAd I and II programs and identifies potential regulators that
307 may differentially regulate the two populations. Motif sequences for Esrrg, Ebf2 and Nr4a2 were
308 highly enriched in ThyAd I, consistent with their significant expression in this population and roles
309 in maintaining a beige-like transcription profile [12,24,59,60]. Both Ebf2 and Esrrg have been
310 demonstrated to promote and maintain a beige/brown transcriptional program [24,61,62]. Esrrg

311 accessibility was mostly restricted to ThyAd Ib in both male and female mice, suggesting Esrrg
312 plays an important role in ThyAd Ib's beige-like transcriptional state. Though *Ebf2* was expressed
313 highly in all clusters, chromatin accessibility displayed a gradient pattern with higher accessibility
314 in ThyAd Is and lower accessibility in ThyAd IIs. Interestingly, though Plagl1 motif accessibility
315 was enriched in ThyAd Is, its expression by RNAseq was increased in ThyAd IIs.

316 ThyAd IIs instead showed increased accessibility for WT1, KLF12, and KLF1. WT1 is
317 known to negatively regulate thermogenic gene expression and beige fat identity [63]. WT1 also
318 modulates EMT/MET during development [64,65]. Interestingly, ThyAd II showed the strongest
319 enrichment for Foxn1 motifs, which were not detected within the RNAseq. This is consistent with
320 a model in which Foxn1 may have been expressed earlier in the etiology of ThyAd II. The origin
321 of adipocytes within the thymic compartment is not well understood. Adipogenesis involves
322 several tightly regulated steps, including the upregulation of PPARγ, a transcriptional factor
323 required for activation of downstream genes [66]. Aire-expressing TECs can give rise to "mimetic"
324 cells that adopt characteristics of peripheral cells including antigens that would not otherwise be
325 found in the thymus. These cells aid in thymic selection and the generation of central tolerance
326 [67]. In humans, Aire deficiency has been associated with Plin-1 autoreactivity and autoimmune
327 adipose infiltration [68,69]. Prior work has identified adipogenic potential in the thymic SVF [70]. These
328 findings suggest that at least a subset of the identified ThyAds may represent an uncharacterized
329 depot of mimetic cells that eluded identification due to their buoyancy. Within the thymus,
330 adipocytes have been suggested to arise from multiple sources, such as infiltration via proximity
331 to the PVS or transdifferentiation from stromal cells with adipogenic potential [71,72]. Lineage tracing
332 experiments using LacZ reporters indicate that at least some adipocytes are derived from Foxn1-
333 expressing TECs [70]. We found that differentially open chromatin in WAT-like ThyAd II nuclei are
334 enriched in binding sites for Foxn1, suggesting that this specific population may emerge from
335 TECs. Other populations Foxn1-negative, EpCAM-negative stromal cells have been identified
336 with adipogenic potential [73]. Together with our findings of multiple distinct ThyAd populations,
337 these findings are most consistent with a complex etiology for ThyAds.

338 We used confocal imaging to identify UCP1+ cells within the thymic parenchyma. These
339 cells were sparse and well-spaced and mostly confined to cortical regions. These findings are
340 consistent with work from Langhi et al., who identified several lipid-laden, Plin1+ populations
341 including preadipocytes, brown adipocytes (UCP1+), macrophages (Iba1+), and pericytes (Ng2+)
342 within the thymic parenchyma, surrounding blood vessels, and the subcapsular zone [22].

343 Thymocyte maturation is dependent on cellular crosstalk within the thymic
344 microenvironment, including between thymic stromal cells and thymocytes. For example, TECs
345 and fibroblasts secrete factors (e.g., IL-7, SCF, DLL4) that drive thymocyte
346 proliferation/differentiation [74]. Reciprocally, thymocytes provide TEC differentiation signals (e.g.,
347 RANKL, CD40, LTβ) to maintain thymic architecture [1]. TEC-derived cells in the thymus are known
348 to play additional roles beyond antigen presentation [75]. More work is required to define ThyAd
349 functions in antigen presentation and other functions such as providing trophic or metabolic
350 support to thymocytes or TECs. Similarly, although ThyAds expand with age their role in thymic
351 involution remains incompletely understood. Injection of T cell progenitors from young mice into
352 aged thymi fails to rescue declining thymopoiesis. Conversely, transplantation of fetal thymic
353 lobes into 18-month-old RAG1$^{-/-}$ mice restores host thymocyte counts to that of 6-8 week-old mice
354 [76]. The fact that other strategies, such as injection of fetal TECs or ectopic expression of Foxn1
355 within adult TECs, only partially rescues aged thymi indicates that multiple attributes intrinsic to
356 aged thymi are responsible for loss of T cell output [77-79]. The possible contribution of one of more
357 ThyAd subsets to this process also awaits experimentation.
358
359 **Limitations of the study**
360 Our findings identify heterogeneity in ThyAds and identify beige-like cells expressing UCP1 within
361 the thymic parenchyma. Although we confined the study to relatively young mice to reduce
362 accumulation of epicardial/perithymic fat which could confound the study, and although thymi
363 were extensively cleaned of fat outside the capsule before processing, it remains formally possible
364 that one or more of the ThyAd subclusters could reflect contamination from perithymic fat, which
365 is known to harbor beige-like cells. It is also possible that one or more subclusters could be
366 molecularly indistinguishable from perithymic fat. Although prior lineage tracing work pinpoints
367 TECs as a source for at least some ThyAds, and although our work is consistent with a TEC origin
368 for ThyAd II, this has not been formally demonstrated. Finally, the study is intended to provide the
369 first molecular ThyAd atlas, and as such contains no information of the functions for these cells in
370 T cell development or thymic involution.

371 **METHOD DETAILS**

372 **Laboratory mice**

373 All mice were C57BL/6J background (#000664, Jackson Laboratories, Bar Harbor, Maine, USA).
374 Mice were housed on a 12h dark/light cycle in groups (maximum five mice per cage) with ad
375 libitum access to water and standard chow diet. All procedures were performed in accordance
376 with the University of Utah Institutional Animal Care and Use Committee (Protocol #00001553).
377

378 **ThyAd isolation**

379 Intact thymi were quickly removed and transferred to a petri dish on ice with ~300uL PBS to keep
380 tissue moist. Thymic capsules were cleaned of directly attached perithymic fat and connective
381 tissues, rinsed a final time with PBS, and transferred to a 15mL conical tube. Digestion Buffer
382 (1mM CaCl2, 250mM sucrose, 1.5mM MgCl2, 10mM KCl, 15mM HEPES, 0.1% BSA) with DNase
383 I (8 μg/mL, D513, Sigma Aldrich) and Collagenase II (2 mg/mL, C1764, Sigma Aldrich) in DMEM-
384 F12 10% FBS was added to each sample and thymi were digested for approximately 10-15
385 minutes at 37°C, horizontally on a shaker set at 300 rpm. Once most of the thymic tissue was
386 digested, an equal volume of FBS was added to each sample to quench the reaction, mixed by
387 gentle pipetting. Samples were fractionated by an initial centrifugation at 300 × *g* at 4°C. The
388 topmost white layer containing mature, floating adipocytes was transferred to a clean 15 mL tube
389 (Figure 1). Then, 10 mL of Wash Buffer (DMEM-F12, 15mM HEPES, 10% FBS) were added to
390 each sample and mixed by gentle inversion and/or trituration with a micropipette to prevent
391 bursting of the adipocytes. Samples were left on ice for 10 min, followed by a second round of
392 centrifugation at 150 × *g* at 4°C. The white floating layer was transferred to a 5 mL conical tube
393 and washed with 4 mL Wash Buffer. Samples were left on ice for 10 min, and spun at 150 × *g* at
394 4°C. The floating fraction was collected and transferred to a clean 1.5 mL eppendorf tube. Without
395 adding more media, samples were centrifuged at 150 *x g* at 4°C. Residual buffer was carefully
396 removed from the bottom of the tube with a 5 mL syringe and 21-gage needle. The remaining
397 white layer of packed adipocytes was transferred to a clean, prechilled 1.5 mL eppendorf tube for
398 nuclei isolation. For the data shown in Figure 4, 6 male thymi were collected, combined, and
399 processed similarly. Gonadal (inguinal) fat (gWAT) was prepared from the same mice in parallel
400 as a quality control.
401

402 **Nuclei and 10X library preparation**

403 To isolate nuclei, samples were incubated with 100 μL 0.1x lysis buffer for 3-5 min on ice as
404 previously described (10X Genomics, Demonstrated Protocol CG000366 Rev D). After washing
405 and centrifugation following the outlined protocol, nuclei were resuspended in diluted 1x Nuclei
406 Buffer (10X Genomics, PN 2000207). The concentration of nuclei was determined by AO/PI using
407 a Luna-FL (Logos Biosystems, Inc., Gyeonggi-do, Korea). Approximately 5,000 nuclei were
408 immediately loaded onto a 10X Next GEM Chip J (10X Genomics, PN 1000230). Single-nuclei
409 libraries were prepared using Chromium Next GEM Single Cell Multiome Reagent Kit A reagents
410 (10X Genomics, PN 1000284) and assessed for quality using an Agilent D1000 ScreenTape.
411 Libraries were sequenced on an Illumina NovaSeq X instrument targeting 100 million paired end
412 reads (GEX) and 300 million paired end reads (ATAC) of 150 bp for each sample.
413
414 **Data analysis**
415 For female thymi, reads were aligned to the *mm10* reference genome (package 2020-A) to
416 generate feature-barcode matrices using cellranger (version 2.0.2). After quality control and
417 thresholding of cellranger output matrices, normalization and PCA of 3,610 high-quality single
418 nuclei was performed in Seurat (v5.1.0) [80]. Sample quality was assessed by joint RNAseq and
419 ATACseq quality control parameters as described in the Seurat WNN and Signac 10x multiomic
420 analysis vignettes [80,81]. Briefly, high-quality nuclei were defined by the number of ATAC transcripts
421 (nCount_ATAC >500 & <70,000), unique genes (nFeature_RNA >200 & <2,500), mitochondrial
422 mRNA content (mt.percent_RNA <20%), nucleosome signal (<2), and TSS enrichment (>1). 3,610
423 nuclei were recovered using this method. Utilizing the Seurat SCTransform pipeline, dimensional
424 reduction (PCA) was performed on the top 3,000 most variable genes. Equivalent normalization
425 of the ATACseq data was performed by latent semantic indexing (LSI). A 'weighted nearest
426 neighbor' (WNN) UMAP was generated using the FindMultiModalNeighbors function, taking both
427 RNAseq and ATACseq datasets into account for subsequent UMAP and cluster visualization.
428 Ptprc-enriched clusters were identified and excluded from downstream analyses while ThyAds
429 were identified as $Ptprc^{lo}$. This operation yielded 429 remaining nuclei. Adipocytes were
430 reclustered using the SCTransform pipeline. Differential gene expression between the newly
431 defined clusters was determined by applying the FindAllMarkers or FindMarkers function, which
432 use a non-parametric Wilcoxon rank sum test with Bonferroni correction on all normalized
433 features. For applicable figures, levels of significance are denoted as $*p < 0.05$, $**p < 0.01$, $***p <$
434 0.001, and $****p < 0.0001$. For male thymi, 4,342 thymic and 4,968 gWAT nuclei were identified
435 in each sample, and following removal of Ptprc-expressing cells 1,521 filtered ThyAd nuclei and

436 3,806 filtered gWAT nuclei were present. Both datasets are hosted on the Gene Expression
437 Omnibus (GEO) server under accession ID GSE319467.
438
439 **Motif, transcription factor, and GO analysis**
440 Motif analysis was performed using chromVAR and additional packages as outlined in the Signac
441 motif analysis and Seurat WNN vignettes [81]. Clusters were compared against each other to
442 identify the topmost differentially accessible motifs (p.val <0.05). To identify transcription factors
443 (TFs) which may underlie ThyAd cluster transcriptional state, TFs with both high differential
444 expression and their corresponding accessible motifs were determined using Seurat's 'presto'
445 package, which uses a Wilcox rank sum test to calculate p-values for both datasets and returning
446 only TFs with p.val <0.01. GO analysis was performed on ThyAd I and ThyAd II cluster DEGs
447 with adjusted p.val <0.05 using the 'fgsea' R package for Biological Process and Hallmark gene
448 sets [82].
449
450 **Immunofluorescence and confocal microscopy**
451 6-month old mice were euthanized by isofluorane and perfused with PBS. Intact thymi and directly
452 attached connective tissue were carefully removed, washed in PBS, and postfixed for 30 min in
453 4% (w/v) paraformaldehyde (PFA). After 3x PBS washes for 20 min each, thymi were incubated
454 in 10% sucrose for 1 hr and then left in 20% sucrose overnight at 4°C. The following day, thymi
455 were incubated in a series of 30% sucrose for at least 2 hr, then incubated in 2:1 OCT
456 compound:20% sucrose for 1 hr. Tissue was embedded in 100% OCT over a dry ice and 2-
457 propanol slurry for sectioning. 10-20 μm cryosections were dried for 40-60 min at 37°C and
458 rehydrated in cold PBS. Tissue was rinsed 3x in PBST (0.1% Tween 20), and permeabilized in
459 PBST for 15 min. Detergent was removed by rinsing 3x in PBS, following which samples were
460 incubated in prewarmed 0.5-1X TrueBlack Lipofluscin Autofluorescence Quencher (Biotium,
461 Fremont, CA) for 2 min. Slides were blocked for 1 hr at RT in PBS containing 10% normal donkey
462 serum, 5% BSA, and 0.2% Triton-X, and incubated overnight in a primary antibody cocktail (10%
463 donkey normal serum, 5% BSA) containing rabbit anti-UCP1 or rabbit anti-PPARγ (Cell Signaling
464 Technologies, MA, USA) at 4°C. Sections were washed in PBS for 20 min thrice, followed by a 2
465 hr incubation with a secondary buffer cocktail at RT (1% BSA, 1:2000 Hoescht 33342, Thermo
466 Fischer Scientific H3570) with or without donkey anti-Alexa Fluor 647 nm (1:400, Invitrogen, La
467 Jolla, CA, USA). Slides were washed and mounted with Fluoromount-G (Thermo Fischer

468 Scientific 00-4958). If substantial TrueBlack was removed from slides after incubation with
469 blocking buffer, the post-staining treatment protocol was used per manufacturer's protocol.
470 Stained sections were imaged by resonance scanning confocal microscopy (A1R confocal system
471 and Eclipse Ti inverted microscope; Nikon, Melville, NY, USA) with a 20X objective and 3X or 8X
472 optical zoom (0.41μm/px).

AUTHOR CONTRIBUTIONS

N.J.S. and D.T. conceived the study. KEV helped with generation of the ThyAd isolation protocol. N.J.S. and A.F. performed experiments. N.J.S. analyzed the data and generated figures. All authors contributed to the writing of the manuscript.

ACKNOWLEDGEMENTS

We thank W.-L. Lo for critical reading of the manuscript. We thank M. Chandrashekharan for help with graphics. We thank B. Dalley, O. Allen and the University of Utah Huntsman Cancer Institute High-Throughput Genomics Core Facility. This work was supported by a pilot grant from the University of Utah Center Diabetes and Metabolism Research Center (DMRC) and an award from the Praespero Foundation (Canada) to D.T.

DECLARATION OF INTERESTS

The authors declare no competing interests.

487 **FIGURE LEGENDS**

488 **Figure 1. Female ThyAds are heterogeneous, with one subclustered harboring**
489 **transcriptional signatures of metabolically active beige fat.**

490 (A) Experimental design for isolation and multiomic sequencing of murine ThyAds. Thymi were
491 processed by mechanical disaggregation, digestion, centrifugation (isolation by buoyancy) and
492 nuclei isolation prior to single-nucleus ATACseq + RNAseq multiomics.

493 (B) Example thymus prior to and after removal of perithymic fat. The septa and thymic lobes were
494 kept intact such that the fatty tissue between the lobes is retained.

495 (C) UMAP projection and clustering of ThyAds by RNAseq, ATACseq, and Weighted Next
496 Neighbor (WNN) analysis. ThyAds (n = 429, avg gene count 2,974) were reclustered after removal
497 of Prprc-expressing nuclei. A residual Ptprc+ cluster was also present.

498 (D) Expression of most distinguishing ThyAd marker genes by cluster. A heatmap displaying the
499 top 10 DEGs within each ThyAd subpopulation is shown.

500

501 **Figure 2. ThyAd I and II display highly differential gene expression.**

502 (A) Violin plots highlighting differential and shared expression of ThyAd I and II cluster-defining
503 genes. Recolored UMAP denotes superclusters Ia/b and Ia/b/c are shown at right.

504 (B) GO Biological Process Analysis for ThyAd Is and II superclusters.

505

506 **Figure 3. Differentially accessible chromatin and transcription factor motif enrichment in**
507 **different ThyAd subpopulations.**

508 (A) Single-nucleus ATAC-seq open chromatin genome tracks at the *Ppara*, *Cidea* and *Ucp1* loci
509 are shown for each subpopulation.

510 (B) Motif analysis comparing combined ThyAd I and II subpopulations. The top 6 most enriched
511 motifs are shown for each grouped population. Asterisks denote motifs unique to that population.

512

513 **Figure 4. Male murine ThyAds are heterogenous and transcriptionally distinct from gWAT.**

514 (A) Experimental design for isolation and multiomic sequencing of murine ThyAds.

515 (B) Single-nucleus RNA-seq UMAPs comparing ThyAds with gWAT isolated from 4-month-old
516 male mice. Nuclei were labeled by tissue.

517 (C) Feature plots showing expression of selected marker genes *Ptprc*, *Pparg*, *Fabp4*, *Adipoq*,
518 *Ppara*, and *Esrrg*.

519 (D) ThyAds were reclustered alone to distinguish 1a, Ib, IIa, IIb, and IIc populations. UMAP feature
520 plots are shown for *Ppara*, *Ghr*, *Ppargc1b*, *Pparg*, *Fabp4*, *Fgf14*, and *Esrrg*.
521
522 **Figure 5. UCP1^{+} cells are detectable in the thymic cortical regions of 6-month-old female**
523 **mice.**
524 (A) Top: 0.8 μm confocal Z-stack images of UCP1 immunofluorescence-stained cryosections of
525 a region of a 6-month-old female murine thymus where the cortex meets the capsule. Slides were
526 counterstained with Hoescht. Dense nuclear stain (blue) denotes the thymic parenchyma,
527 predominantly TECs and thymocytes. Intense UCP1 staining is present in perithymic fat attached
528 to the thymic capsule with a distinct expression pattern compared to scattered parenchymal
529 UCP1+ cells (highlighted with yellow arrows). At right is shown a higher magnification image of
530 the same slide. Bottom: an adjacent cryosection stained and imaged identically except lacking
531 the primary antibody.
532 (B) Similarly processed images of a different section from the same thymus.
533
534 **SUPPLEMENTAL FIGURE LEGENDS**
535 **Supplemental Figure 1. Quality control for single-nucleus ATAC-seq plus RNA-seq**
536 **multiomics.**
537 (A) example nuclei following isolation. Areas of heterochromatin are preserved.
538 (B) Thresholding and quality control parameters employed to eliminate low-quality nuclei. Left:
539 mitochondrial regression/normalization. Removed nuclei are shown in gray (top left). Right:
540 Density plot showing retained nuclei by TSS enrichment and total peak fragments. nCount_ATAC
541 quantiles are: 5% 6438.45; 10% 7834; 90% 29520.1. TSS. Enrichment quantiles are: 5% 5.47;
542 10% 5.8; 95% 8.96.
543 (C) WNN UMAP clustering of 3,610 nuclei isolated from the floating fraction of female 6-month
544 old thymic tissue. Clusters 3 and 10 are highlighted (red circles) and identified as Ptprc^{lo} and
545 Pparg^{+}Plin1^{+}. This subset was used for further downstream analysis.
546 (D) Selected marker genes used to identify immune populations and adipocytes are shown as
547 violin plots by cluster.
548
549 **Supplemental Figure 2. Lipid-metabolism-related gene expression comparing whole**
550 **sample and ThyAds.**

551 (A) Dot Plots of whole sample ThyAds showing expression of genes associated with lipid
552 metabolism. Genes associated with lipogenesis (*Fasn*, *Acaca*, *Elovl6*, *Dgat1*, *Dgat2*, *Srebf1*, *Acly*,
553 *Scd1*, *Scd1*) and lipolysis (*Lipe*, *Pnpla2*, *Mgll*, *Gk*, *Abhd5*) are shown.
554 (B) The same analysis was performed for subsetted Pparg+Fabp4+Plin1+ ThyAds and the
555 residual Ptprc+ cluster.
556
557 **Supplemental Figure 3. Expression of selected markers by ThyAds and top DEGs by**
558 **cluster.**
559 (A) Heatmap displaying the top 10 DEGs for cluster including the Ptprc+ nuclei.
560 (B) WNN UMAP projections of genes encoding selected adipokines (*Adipoq*, *Retn*, *Lep*, *Cfd*) and
561 beige/brown adipocyte marker genes (*Cidea*, *Prdm16*, *Ucp1*, *Esrrg*, *Ppargc1a*, *Ppargc1b*). *Plin1*,
562 *Fasn*, *Ebf2*, *Zfp423*, *Col15a1*, *Aldh1a1*, *Prr16* and *Rems3* are also shown.
563
564 **Supplemental Figure 4. Gene expression and open chromatin states of potential ThyAd**
565 **transcription regulators.**
566 (A) Feature plots of WNN UMAPS showing expression and chromatin accessibility for additional
567 genes. *Ebf2*, *Esrrg*, *Plagl1*, and *Foxn1* are shown. Gene expression plots for *Foxn1* could not be
568 generated because Foxn1 was not expressed in any nucleus. The WNN plot from Figure 1C is
569 recapitulated at right for comparison.
570 (B) Single-nucleus ATAC-seq open chromatin genome tracks at the *Foxn1* locus is shown for
571 each subpopulation.
572
573 **Supplemental Figure 5. Gene expression differences associated with ThyAd and gWAT**
574 **tissue from 4-month-old male mice.**
575 (A) Heatmap displaying the top 10 DEGs within each ThyAd and gWAT subpopulation is shown.
576 (B) Similar to Figure 4C except additional genes are shown: *Ebf2*, *Cidea*, *Prdm16*, *Ghr*, *Ebf1*, and
577 *Aifm2*.
578
579 **Supplemental Figure 6. PPARγ-positive cells identified within the thymus.**
580 IF image of a 16 μm cryosection of a thymus from a 6-month-old female mouse. Samples was
581 stained with BODIPY (488 nm), rabbit anti-PPARγ (647 nm) and Hoescht (405 nm).

582 **REFERENCES**

583

584 1. Li, Y.R., and Zuniga-Pflucker, J.C. (2023). Thymus aging and immune reconstitution,
585 progresses and challenges. Semin Immunol *70*, 101837. 10.1016/j.smim.2023.101837.
586 2. Lynch, H.E., Goldberg, G.L., Chidgey, A., Van den Brink, M.R., Boyd, R., and
587 Sempowski, G.D. (2009). Thymic involution and immune reconstitution. Trends Immunol
588 *30*, 366-373. 10.1016/j.it.2009.04.003.
589 3. Min, H., Montecino-Rodriguez, E., and Dorshkind, K. (2004). Reduction in the
590 developmental potential of intrathymic T cell progenitors with age. J Immunol *173*, 245-
591 250. 10.4049/jimmunol.173.1.245.
592 4. Cisneros, B., Garcia-Aguirre, I., Unzueta, J., Arrieta-Cruz, I., Gonzalez-Morales, O.,
593 Dominguez-Larrieta, J.M., Tamez-Gonzalez, A., Leyva-Gomez, G., and Magana, J.J.
594 (2022). Immune system modulation in aging: Molecular mechanisms and therapeutic
595 targets. Front Immunol *13*, 1059173. 10.3389/fimmu.2022.1059173.
596 5. Weng, N.P., Akbar, A.N., and Goronzy, J. (2009). CD28(-) T cells: their role in the age-
597 associated decline of immune function. Trends Immunol *30*, 306-312.
598 10.1016/j.it.2009.03.013.
599 6. Saurwein-Teissl, M., Lung, T.L., Marx, F., Gschosser, C., Asch, E., Blasko, I., Parson,
600 W., Bock, G., Schonitzer, D., Trannoy, E., and Grubeck-Loebenstein, B. (2002). Lack of
601 antibody production following immunization in old age: association with CD8(+)CD28(-) T
602 cell clonal expansions and an imbalance in the production of Th1 and Th2 cytokines. J
603 Immunol *168*, 5893-5899. 10.4049/jimmunol.168.11.5893.
604 7. Dorshkind, K., and Swain, S. (2009). Age-associated declines in immune system
605 development and function: causes, consequences, and reversal. Curr Opin Immunol *21*,
606 404-407. 10.1016/j.coi.2009.07.001.
607 8. Youm, Y.H., Yang, H., Amin, R., Smith, S.R., Leff, T., and Dixit, V.D. (2010).
608 Thiazolidinedione treatment and constitutive-PPARgamma activation induces ectopic
609 adipogenesis and promotes age-related thymic involution. Aging Cell *9*, 478-489.
610 10.1111/j.1474-9726.2010.00574.x.
611 9. Laan, M., Haljasorg, U., Kisand, K., Salumets, A., and Peterson, P. (2016). Pregnancy-
612 induced thymic involution is associated with suppression of chemokines essential for T-
613 lymphoid progenitor homing. Eur J Immunol *46*, 2008-2017. 10.1002/eji.201646309.
614 10. Billard, M.J., Gruver, A.L., and Sempowski, G.D. (2011). Acute endotoxin-induced
615 thymic atrophy is characterized by intrathymic inflammatory and wound healing
616 responses. PLoS One *6*, e17940. 10.1371/journal.pone.0017940.
617 11. Howard, J.K., Lord, G.M., Matarese, G., Vendetti, S., Ghatei, M.A., Ritter, M.A., Lechler,
618 R.I., and Bloom, S.R. (1999). Leptin protects mice from starvation-induced lymphoid
619 atrophy and increases thymic cellularity in ob/ob mice. J Clin Invest *104*, 1051-1059.
620 10.1172/JCI6762.
621 12. Emont, M.P., Jacobs, C., Essene, A.L., Pant, D., Tenen, D., Colleluori, G., Di Vincenzo,
622 A., Jorgensen, A.M., Dashti, H., Stefek, A., et al. (2022). A single-cell atlas of human and
623 mouse white adipose tissue. Nature *603*, 926-933. 10.1038/s41586-022-04518-2.
624 13. Bautista, J.L., Cramer, N.T., Miller, C.N., Chavez, J., Berrios, D.I., Byrnes, L.E.,
625 Germino, J., Ntranos, V., Sneddon, J.B., Burt, T.D., et al. (2021). Single-cell
626 transcriptional profiling of human thymic stroma uncovers novel cellular heterogeneity in
627 the thymic medulla. Nat Commun *12*, 1096. 10.1038/s41467-021-21346-6.
628 14. Cordes, M., Cante-Barrett, K., van den Akker, E.B., Moretti, F.A., Kielbasa, S.M.,
629 Vloemans, S.A., Garcia-Perez, L., Teodosio, C., van Dongen, J.J.M., Pike-Overzet, K.,

et al. (2022). Single-cell immune profiling reveals thymus-seeding populations, T cell commitment, and multilineage development in the human thymus. Sci Immunol *7*, eade0182. 10.1126/sciimmunol.ade0182.

15. Lavaert, M., Liang, K.L., Vandamme, N., Park, J.E., Roels, J., Kowalczyk, M.S., Li, B., Ashenberg, O., Tabaka, M., Dionne, D., et al. (2020). Integrated scRNA-Seq Identifies Human Postnatal Thymus Seeding Progenitors and Regulatory Dynamics of Differentiating Immature Thymocytes. Immunity *52*, 1088-1104 e1086. 10.1016/j.immuni.2020.03.019.
16. Le, J., Park, J.E., Ha, V.L., Luong, A., Branciamore, S., Rodin, A.S., Gogoshin, G., Li, F., Loh, Y.E., Camacho, V., et al. (2020). Single-Cell RNA-Seq Mapping of Human Thymopoiesis Reveals Lineage Specification Trajectories and a Commitment Spectrum in T Cell Development. Immunity *52*, 1105-1118 e1109. 10.1016/j.immuni.2020.05.010.
17. Gabriely, I., Ma, X.H., Yang, X.M., Atzmon, G., Rajala, M.W., Berg, A.H., Scherer, P., Rossetti, L., and Barzilai, N. (2002). Removal of visceral fat prevents insulin resistance and glucose intolerance of aging: an adipokine-mediated process? Diabetes *51*, 2951-2958. 10.2337/diabetes.51.10.2951.
18. Huh, J.Y., Park, J., Kim, J.I., Park, Y.J., Lee, Y.K., and Kim, J.B. (2017). Deletion of CD1d in Adipocytes Aggravates Adipose Tissue Inflammation and Insulin Resistance in Obesity. Diabetes *66*, 835-847. 10.2337/db16-1122.
19. Zoico, E., Rubele, S., De Caro, A., Nori, N., Mazzali, G., Fantin, F., Rossi, A., and Zamboni, M. (2019). Brown and Beige Adipose Tissue and Aging. Front Endocrinol (Lausanne) *10*, 368. 10.3389/fendo.2019.00368.
20. Porter, J.W., Barnas, J.L., Welly, R., Spencer, N., Pitt, J., Vieira-Potter, V.J., and Kanaley, J.A. (2020). Age, Sex, and Depot-Specific Differences in Adipose-Tissue Estrogen Receptors in Individuals with Obesity. Obesity (Silver Spring) *28*, 1698-1707. 10.1002/oby.22888.
21. Varghese, M., Song, J., and Singer, K. (2021). Age and Sex: Impact on adipose tissue metabolism and inflammation. Mech Ageing Dev *199*, 111563. 10.1016/j.mad.2021.111563.
22. Langhi, L.G., Andrade, L.R., Shimabukuro, M.K., van Ewijk, W., Taub, D.D., Borojevic, R., and de Mello Coelho, V. (2015). Lipid-Laden Multilocular Cells in the Aging Thymus Are Phenotypically Heterogeneous. PLoS One *10*, e0141516. 10.1371/journal.pone.0141516.
23. Dixen, K., Basse, A.L., Murholm, M., Isidor, M.S., Hansen, L.H., Petersen, M.C., Madsen, L., Petrovic, N., Nedergaard, J., Quistorff, B., and Hansen, J.B. (2013). ERRgamma enhances UCP1 expression and fatty acid oxidation in brown adipocytes. Obesity (Silver Spring) *21*, 516-524. 10.1002/oby.20067.
24. Muller, S., Perdikari, A., Dapito, D.H., Sun, W., Wollscheid, B., Balaz, M., and Wolfrum, C. (2020). ESRRG and PERM1 Govern Mitochondrial Conversion in Brite/Beige Adipocyte Formation. Front Endocrinol (Lausanne) *11*, 387. 10.3389/fendo.2020.00387.
25. Jash, S., Banerjee, S., Lee, M.J., Farmer, S.R., and Puri, V. (2019). CIDEA Transcriptionally Regulates UCP1 for Britening and Thermogenesis in Human Fat Cells. iScience *20*, 73-89. 10.1016/j.isci.2019.09.011.
26. Montoya, M., and Del Val, M. (1999). Intracellular rate-limiting steps in MHC class I antigen processing. J Immunol *163*, 1914-1922.
27. Kousa, A.I., Jahn, L., Zhao, K., Flores, A.E., Acenas, D., 2nd, Lederer, E., Argyropoulos, K.V., Lemarquis, A.L., Granadier, D., Cooper, K., et al. (2024). Age-related epithelial defects limit thymic function and regeneration. Nat Immunol *25*, 1593-1606. 10.1038/s41590-024-01915-9.

679 28. Seale, P., Kajimura, S., Yang, W., Chin, S., Rohas, L.M., Uldry, M., Tavernier, G.,
680 Langin, D., and Spiegelman, B.M. (2007). Transcriptional control of brown fat
681 determination by PRDM16. Cell Metab *6*, 38-54. 10.1016/j.cmet.2007.06.001.
682 29. Hinds, T.D., Jr., Kipp, Z.A., Xu, M., Yiannikouris, F.B., Morris, A.J., Stec, D.F., Wahli, W.,
683 and Stec, D.E. (2021). Adipose-Specific PPARalpha Knockout Mice Have Increased
684 Lipogenesis by PASK-SREBP1 Signaling and a Polarity Shift to Inflammatory
685 Macrophages in White Adipose Tissue. Cells *11*. 10.3390/cells11010004.
686 30. Holman, C.D., Sakers, A.P., Calhoun, R.P., Cheng, L., Fein, E.C., Jacobs, C., Tsai, L.,
687 Rosen, E.D., and Seale, P. (2024). Aging impairs cold-induced beige adipogenesis and
688 adipocyte metabolic reprogramming. bioRxiv. 10.1101/2023.03.20.533514.
689 31. Kim, K.H., Lee, K., Moon, Y.S., and Sul, H.S. (2001). A cysteine-rich adipose tissue-
690 specific secretory factor inhibits adipocyte differentiation. J Biol Chem *276*, 11252-
691 11256. 10.1074/jbc.C100028200.
692 32. Nehls, M., Kyewski, B., Messerle, M., Waldschutz, R., Schuddekopf, K., Smith, A.J., and
693 Boehm, T. (1996). Two genetically separable steps in the differentiation of thymic
694 epithelium. Science *272*, 886-889. 10.1126/science.272.5263.886.
695 33. Simpson, J.G., Gray, E.S., and Beck, J.S. (1975). Age involution in the normal human
696 adult thymus. Clin Exp Immunol *19*, 261-265.
697 34. Pido-Lopez, J., Imami, N., and Aspinall, R. (2001). Both age and gender affect thymic
698 output: more recent thymic migrants in females than males as they age. Clin Exp
699 Immunol *125*, 409-413. 10.1046/j.1365-2249.2001.01640.x.
700 35. Sandstedt, M., Chung, R.W.S., Skoglund, C., Lundberg, A.K., Ostgren, C.J., Ernerudh,
701 J., and Jonasson, L. (2023). Complete fatty degeneration of thymus associates with
702 male sex, obesity and loss of circulating naive CD8(+) T cells in a Swedish middle-aged
703 population. Immun Ageing *20*, 45. 10.1186/s12979-023-00371-7.
704 36. Baran-Gale, J., Morgan, M.D., Maio, S., Dhalla, F., Calvo-Asensio, I., Deadman, M.E.,
705 Handel, A.E., Maynard, A., Chen, S., Green, F., et al. (2020). Ageing compromises
706 mouse thymus function and remodels epithelial cell differentiation. Elife *9*.
707 10.7554/eLife.56221.
708 37. Flores, K.G., Li, J., Sempowski, G.D., Haynes, B.F., and Hale, L.P. (1999). Analysis of
709 the human thymic perivascular space during aging. J Clin Invest *104*, 1031-1039.
710 10.1172/JCI7558.
711 38. Kumar, R., Langer, J.C., and Snoeck, H.W. (2006). Transforming growth factor-beta2 is
712 involved in quantitative genetic variation in thymic involution. Blood *107*, 1974-1979.
713 10.1182/blood-2005-04-1495.
714 39. Frontini, A., Rousset, S., Cassard-Doulcier, A.M., Zingaretti, C., Ricquier, D., and Cinti,
715 S. (2007). Thymus uncoupling protein 1 is exclusive to typical brown adipocytes and is
716 not found in thymocytes. J Histochem Cytochem *55*, 183-189. 10.1369/jhc.6A7013.2006.
717 40. Aw, D., Silva, A.B., Maddick, M., von Zglinicki, T., and Palmer, D.B. (2008). Architectural
718 changes in the thymus of aging mice. Aging Cell *7*, 158-167. 10.1111/j.1474-
719 9726.2007.00365.x.
720 41. Angueira, A.R., Sakers, A.P., Holman, C.D., Cheng, L., Arbocco, M.N., Shamsi, F.,
721 Lynes, M.D., Shrestha, R., Okada, C., Batmanov, K., et al. (2021). Defining the lineage
722 of thermogenic perivascular adipose tissue. Nat Metab *3*, 469-484. 10.1038/s42255-021-
723 00380-0.
724 42. Shao, M., Hepler, C., Vishvanath, L., MacPherson, K.A., Busbuso, N.C., and Gupta,
725 R.K. (2017). Fetal development of subcutaneous white adipose tissue is dependent on
726 Zfp423. Mol Metab *6*, 111-124. 10.1016/j.molmet.2016.11.009.

727 43. Trayhurn, P., and Wood, I.S. (2004). Adipokines: inflammation and the pleiotropic role of
728 white adipose tissue. Br J Nutr *92*, 347-355. 10.1079/bjn20041213.
729 44. Lynch, L., Nowak, M., Varghese, B., Clark, J., Hogan, A.E., Toxavidis, V., Balk, S.P.,
730 O'Shea, D., O'Farrelly, C., and Exley, M.A. (2012). Adipose tissue invariant NKT cells
731 protect against diet-induced obesity and metabolic disorder through regulatory cytokine
732 production. Immunity *37*, 574-587. 10.1016/j.immuni.2012.06.016.
733 45. Cawthorn, W.P., Scheller, E.L., and MacDougald, O.A. (2012). Adipose tissue stem cells
734 meet preadipocyte commitment: going back to the future. J Lipid Res *53*, 227-246.
735 10.1194/jlr.R021089.
736 46. Braissant, O., Foufelle, F., Scotto, C., Dauca, M., and Wahli, W. (1996). Differential
737 expression of peroxisome proliferator-activated receptors (PPARs): tissue distribution of
738 PPAR-alpha, -beta, and -gamma in the adult rat. Endocrinology *137*, 354-366.
739 10.1210/endo.137.1.8536636.
740 47. Peeters, A., and Baes, M. (2010). Role of PPARalpha in Hepatic Carbohydrate
741 Metabolism. PPAR Res *2010*. 10.1155/2010/572405.
742 48. Kersten, S., Seydoux, J., Peters, J.M., Gonzalez, F.J., Desvergne, B., and Wahli, W.
743 (1999). Peroxisome proliferator-activated receptor alpha mediates the adaptive response
744 to fasting. J Clin Invest *103*, 1489-1498. 10.1172/JCI6223.
745 49. Kroon, T., Harms, M., Maurer, S., Bonnet, L., Alexandersson, I., Lindblom, A., Ahnmark,
746 A., Nilsson, D., Gennemark, P., O'Mahony, G., et al. (2020). PPARgamma and
747 PPARalpha synergize to induce robust browning of white fat in vivo. Mol Metab *36*,
748 100964. 10.1016/j.molmet.2020.02.007.
749 50. Kissig, M., Ishibashi, J., Harms, M.J., Lim, H.W., Stine, R.R., Won, K.J., and Seale, P.
750 (2017). PRDM16 represses the type I interferon response in adipocytes to promote
751 mitochondrial and thermogenic programing. EMBO J *36*, 1528-1542.
752 10.15252/embj.201695588.
753 51. Peverelli, E., Ermetici, F., Corbetta, S., Gozzini, E., Avagliano, L., Zappa, M.A.,
754 Bulfamante, G., Beck-Peccoz, P., Spada, A., and Mantovani, G. (2013). PKA regulatory
755 subunit R2B is required for murine and human adipocyte differentiation. Endocr Connect
756 *2*, 196-207. 10.1530/EC-13-0049.
757 52. Harms, M.J., Ishibashi, J., Wang, W., Lim, H.W., Goyama, S., Sato, T., Kurokawa, M.,
758 Won, K.J., and Seale, P. (2014). Prdm16 is required for the maintenance of brown
759 adipocyte identity and function in adult mice. Cell Metab *19*, 593-604.
760 10.1016/j.cmet.2014.03.007.
761 53. Ellis, J.M., Li, L.O., Wu, P.C., Koves, T.R., Ilkayeva, O., Stevens, R.D., Watkins, S.M.,
762 Muoio, D.M., and Coleman, R.A. (2010). Adipose acyl-CoA synthetase-1 directs fatty
763 acids toward beta-oxidation and is required for cold thermogenesis. Cell Metab *12*, 53-
764 64. 10.1016/j.cmet.2010.05.012.
765 54. Kang, G.J., Park, J.H., Kim, H.J., Kim, E.J., Kim, B., Byun, H.J., Yu, L., Nguyen, T.M.,
766 Nguyen, T.H., Kim, K.S., et al. (2022). PRR16/Largen Induces Epithelial-Mesenchymal
767 Transition through the Interaction with ABI2 Leading to the Activation of ABL1 Kinase.
768 Biomol Ther (Seoul) *30*, 340-347. 10.4062/biomolther.2022.066.
769 55. Monteiro, M.C., Sanyal, M., Cleary, M.L., Sengenes, C., Bouloumie, A., Dani, C., and
770 Billon, N. (2011). PBX1: a novel stage-specific regulator of adipocyte development. Stem
771 Cells *29*, 1837-1848. 10.1002/stem.737.
772 56. Xia, T., Shen, Z., Cai, J., Pan, M., and Sun, C. (2020). ColXV Aggravates Adipocyte
773 Apoptosis by Facilitating Abnormal Extracellular Matrix Remodeling in Mice. Int J Mol Sci
774 *21*. 10.3390/ijms21030959.

775 57. Zhu, X., Wei, L., Bai, Y., Wu, S., and Han, S. (2017). FoxC1 promotes epithelial-
776 mesenchymal transition through PBX1 dependent transactivation of ZEB2 in esophageal
777 cancer. Am J Cancer Res *7*, 1642-1653.
778 58. Lambert, A.W., and Weinberg, R.A. (2021). Linking EMT programmes to normal and
779 neoplastic epithelial stem cells. Nat Rev Cancer *21*, 325-338. 10.1038/s41568-021-
780 00332-6.
781 59. Roh, H.C., Tsai, L.T.Y., Shao, M., Tenen, D., Shen, Y., Kumari, M., Lyubetskaya, A.,
782 Jacobs, C., Dawes, B., Gupta, R.K., and Rosen, E.D. (2018). Warming Induces
783 Significant Reprogramming of Beige, but Not Brown, Adipocyte Cellular Identity. Cell
784 Metab *27*, 1121-1137 e1125. 10.1016/j.cmet.2018.03.005.
785 60. Lee, S., Benvie, A.M., Park, H.G., Spektor, R., Harlan, B., Brenna, J.T., Berry, D.C., and
786 Soloway, P.D. (2022). Remodeling of gene regulatory networks underlying thermogenic
787 stimuli-induced adipose beiging. Commun Biol *5*, 584. 10.1038/s42003-022-03531-5.
788 61. Rajakumari, S., Wu, J., Ishibashi, J., Lim, H.W., Giang, A.H., Won, K.J., Reed, R.R., and
789 Seale, P. (2013). EBF2 determines and maintains brown adipocyte identity. Cell Metab
790 *17*, 562-574. 10.1016/j.cmet.2013.01.015.
791 62. Brown, E.L., Hazen, B.C., Eury, E., Wattez, J.S., Gantner, M.L., Albert, V., Chau, S.,
792 Sanchez-Alavez, M., Conti, B., and Kralli, A. (2018). Estrogen-Related Receptors
793 Mediate the Adaptive Response of Brown Adipose Tissue to Adrenergic Stimulation.
794 iScience *2*, 221-237. 10.1016/j.isci.2018.03.005.
795 63. Kirschner, K.M., Foryst-Ludwig, A., Gohlke, S., Li, C., Flores, R.E., Kintscher, U.,
796 Schupp, M., Schulz, T.J., and Scholz, H. (2022). Wt1 haploinsufficiency induces
797 browning of epididymal fat and alleviates metabolic dysfunction in mice on high-fat diet.
798 Diabetologia *65*, 528-540. 10.1007/s00125-021-05621-1.
799 64. Martinez-Estrada, O.M., Lettice, L.A., Essafi, A., Guadix, J.A., Slight, J., Velecela, V.,
800 Hall, E., Reichmann, J., Devenney, P.S., Hohenstein, P., et al. (2010). Wt1 is required
801 for cardiovascular progenitor cell formation through transcriptional control of Snail and E-
802 cadherin. Nat Genet *42*, 89-93. 10.1038/ng.494.
803 65. Essafi, A., Webb, A., Berry, R.L., Slight, J., Burn, S.F., Spraggon, L., Velecela, V.,
804 Martinez-Estrada, O.M., Wiltshire, J.H., Roberts, S.G., et al. (2011). A wt1-controlled
805 chromatin switching mechanism underpins tissue-specific wnt4 activation and
806 repression. Dev Cell *21*, 559-574. 10.1016/j.devcel.2011.07.014.
807 66. Tontonoz, P., Hu, E., and Spiegelman, B.M. (1994). Stimulation of adipogenesis in
808 fibroblasts by PPAR gamma 2, a lipid-activated transcription factor. Cell *79*, 1147-1156.
809 10.1016/0092-8674(94)90006-x.
810 67. Michelson, D.A., Hase, K., Kaisho, T., Benoist, C., and Mathis, D. (2022). Thymic
811 epithelial cells co-opt lineage-defining transcription factors to eliminate autoreactive T
812 cells. Cell *185*, 2542-2558 e2518. 10.1016/j.cell.2022.05.018.
813 68. Mandel-Brehm, C., Vazquez, S.E., Liverman, C., Cheng, M., Quandt, Z., Kung, A.F.,
814 Parent, A., Miao, B., Disse, E., Cugnet-Anceau, C., et al. (2023). Autoantibodies to
815 Perilipin-1 Define a Subset of Acquired Generalized Lipodystrophy. Diabetes *72*, 59-70.
816 10.2337/db21-1172.
817 69. Agarwal, S., Bodansky, A., Xing, C., Anderson, M.S., and Garg, A. (2024). Partial
818 Lipodystrophy Affecting the Extremities in a Young Woman With Autoimmune
819 Polyglandular Syndrome 1. JCEM Case Rep *2*, luae166. 10.1210/jcemcr/luae166.
820 70. Youm, Y.H., Yang, H., Sun, Y., Smith, R.G., Manley, N.R., Vandanmagsar, B., and Dixit,
821 V.D. (2009). Deficient ghrelin receptor-mediated signaling compromises thymic stromal
822 cell microenvironment by accelerating thymic adiposity. J Biol Chem *284*, 7068-7077.
823 10.1074/jbc.M808302200.

824 71. Yang, H., Youm, Y.H., Sun, Y., Rim, J.S., Galban, C.J., Vandanmagsar, B., and Dixit,
825 V.D. (2009). Axin expression in thymic stromal cells contributes to an age-related
826 increase in thymic adiposity and is associated with reduced thymopoiesis independently
827 of ghrelin signaling. J Leukoc Biol *85*, 928-938. 10.1189/jlb.1008621.
828 72. Yang, H., Youm, Y.H., Vandanmagsar, B., Rood, J., Kumar, K.G., Butler, A.A., and Dixit,
829 V.D. (2009). Obesity accelerates thymic aging. Blood *114*, 3803-3812. 10.1182/blood-
830 2009-03-213595.
831 73. Sheridan, J.M., Keown, A., Policheni, A., Roesley, S.N.A., Rivlin, N., Kadouri, N.,
832 Ritchie, M.E., Jain, R., Abramson, J., Heng, T.S.P., and Gray, D.H.D. (2017).
833 Thymospheres Are Formed by Mesenchymal Cells with the Potential to Generate
834 Adipocytes, but Not Epithelial Cells. Cell Rep *21*, 934-942.
835 10.1016/j.celrep.2017.09.090.
836 74. Venables, T., Griffith, A.V., DeAraujo, A., and Petrie, H.T. (2019). Dynamic changes in
837 epithelial cell morphology control thymic organ size during atrophy and regeneration. Nat
838 Commun *10*, 4402. 10.1038/s41467-019-11879-2.
839 75. Givony, T., Leshkowitz, D., Del Castillo, D., Nevo, S., Kadouri, N., Dassa, B., Gruper, Y.,
840 Khalaila, R., Ben-Nun, O., Gome, T., et al. (2023). Thymic mimetic cells function beyond
841 self-tolerance. Nature *622*, 164-172. 10.1038/s41586-023-06512-8.
842 76. Zhu, X., Gui, J., Dohkan, J., Cheng, L., Barnes, P.F., and Su, D.M. (2007).
843 Lymphohematopoietic progenitors do not have a synchronized defect with age-related
844 thymic involution. Aging Cell *6*, 663-672. 10.1111/j.1474-9726.2007.00325.x.
845 77. Oh, J., Wang, W., Thomas, R., and Su, D.M. (2020). Thymic rejuvenation via FOXN1-
846 reprogrammed embryonic fibroblasts (FREFs) to counteract age-related inflammation.
847 JCI Insight *5*. 10.1172/jci.insight.140313.
848 78. Kim, M.J., Miller, C.M., Shadrach, J.L., Wagers, A.J., and Serwold, T. (2015). Young,
849 proliferative thymic epithelial cells engraft and function in aging thymuses. J Immunol
850 *194*, 4784-4795. 10.4049/jimmunol.1403158.
851 79. Bredenkamp, N., Nowell, C.S., and Blackburn, C.C. (2014). Regeneration of the aged
852 thymus by a single transcription factor. Development *141*, 1627-1637.
853 10.1242/dev.103614.
854 80. Stuart, T., Butler, A., Hoffman, P., Hafemeister, C., Papalexi, E., Mauck, W.M., 3rd, Hao,
855 Y., Stoeckius, M., Smibert, P., and Satija, R. (2019). Comprehensive Integration of
856 Single-Cell Data. Cell *177*, 1888-1902 e1821. 10.1016/j.cell.2019.05.031.
857 81. Stuart, T., Srivastava, A., Madad, S., Lareau, C.A., and Satija, R. (2021). Single-cell
858 chromatin state analysis with Signac. Nat Methods *18*, 1333-1341. 10.1038/s41592-021-
859 01282-5.
860 82. Sergushichev, A.A. (2016). An algorithm for fast preranked gene set enrichment analysis
861 using cumulative statistic calculation. bioRxiv *060012*. https://doi.org/10.1101/060012.
862

Figure 1

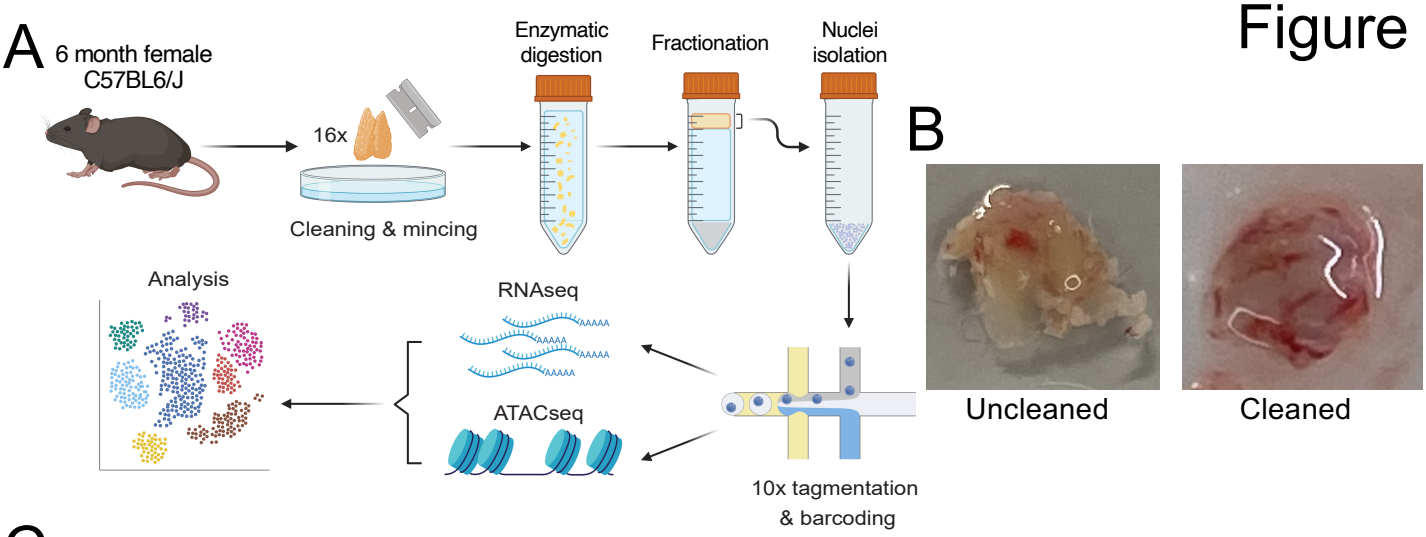
A
6 month female
C57BL6/J
16x
Cleaning & mincing
Enzymatic digestion
Fractionation
Nuclei isolation
Analysis
RNAseq
ATACseq
10x tagmentation & barcoding
B
Uncleaned
Cleaned

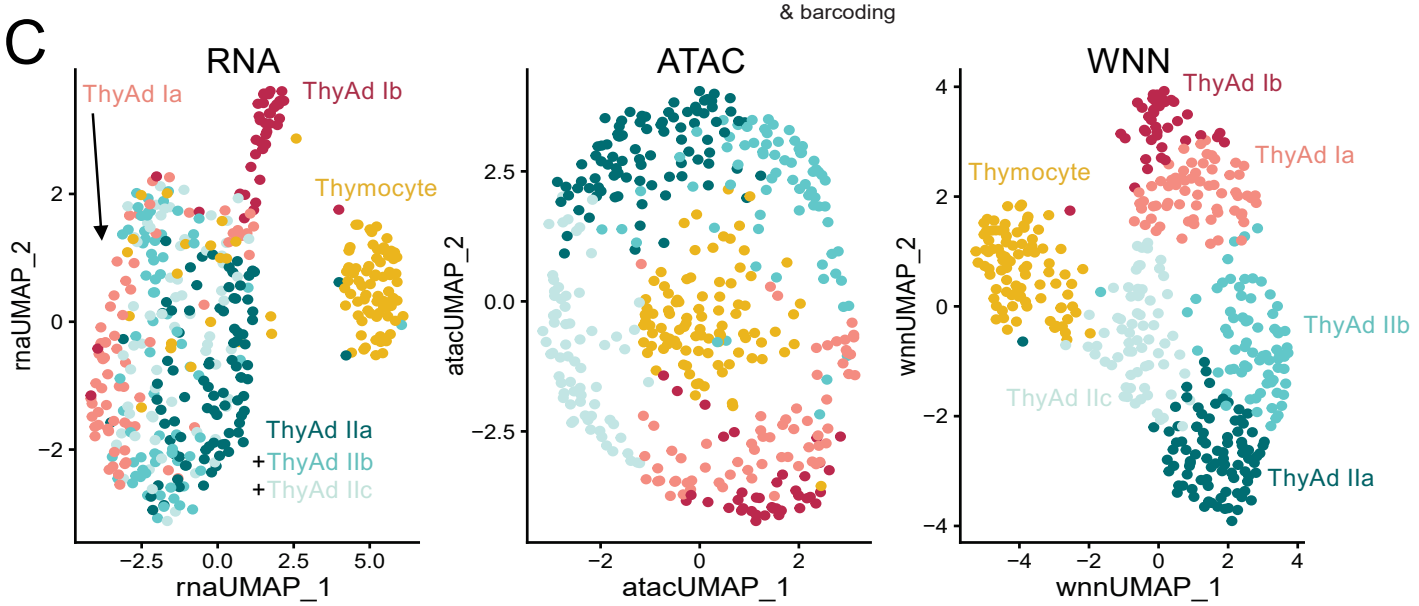
C
RNA
ATAC
WNN
ThyAd Ia
ThyAd Ib
Thymocyte
ThyAd IIa
+ThyAd IIb
+ThyAd IIc
ThyAd IIb
ThyAd IIc
rnaUMAP_1
rnaUMAP_2
atacUMAP_1
atacUMAP_2
wnnUMAP_1
wnnUMAP_2

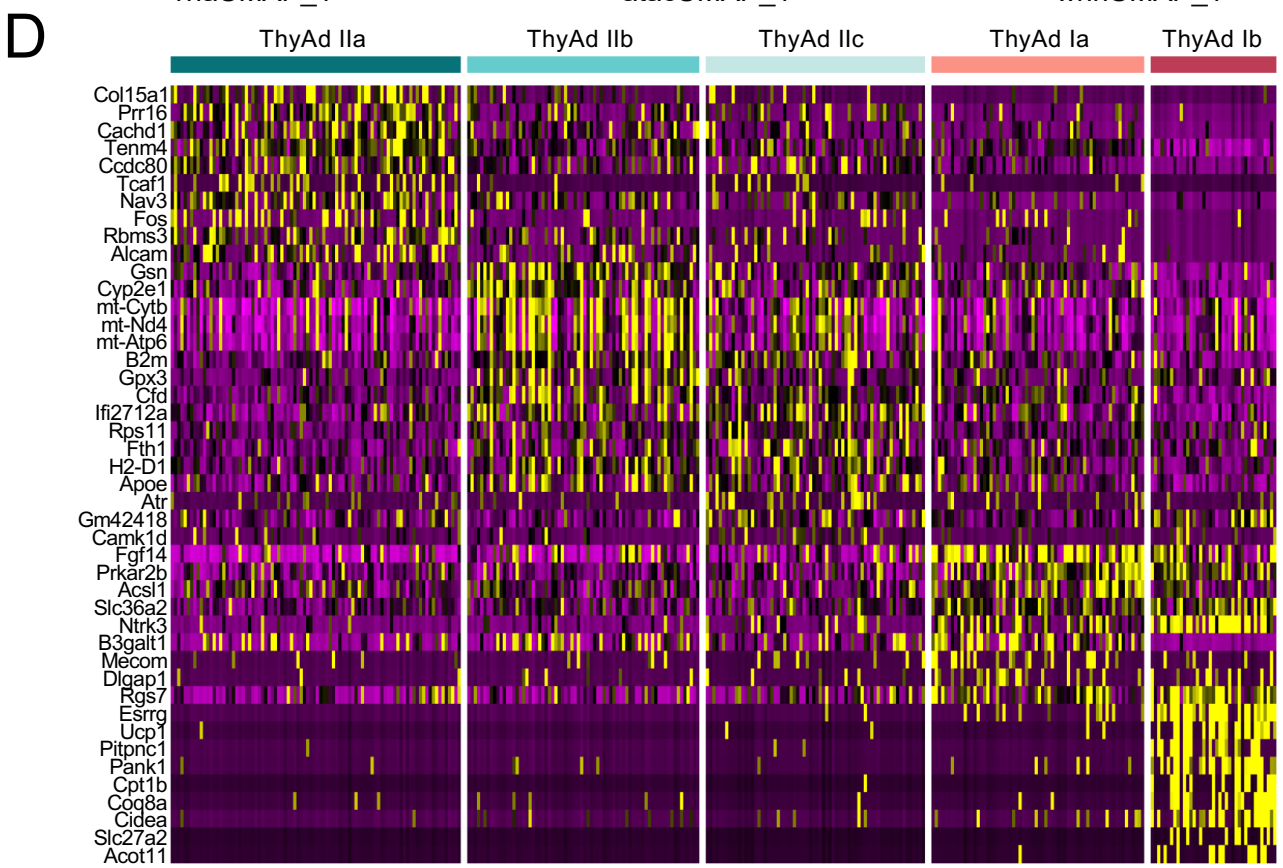
D
ThyAd IIa
ThyAd IIb
ThyAd IIc
ThyAd Ia
ThyAd Ib
Col15a1
Prr16
Cachd1
Tenm4
Ccdc80
Tcaf1
Nav3
Fos
Rbms3
Alcam
Gsn
Cyp2e1
mt-Cytb
mt-Nd4
mt-Atp6
B2m
Gpx3
Cfd
Ifi2712a
Rps11
Fth1
H2-D1
Apoe
Atr
Gm42418
Camk1d
Fgf14
Prkar2b
Acsl1
Slc36a2
Ntrk3
B3galt1
Mecom
Dlgap1
Rgs7
Esrrg
Ucp1
Pitpnc1
Pank1
Cpt1b
Coq8a
Cidea
Slc27a2
Acot11

Figure 2

A

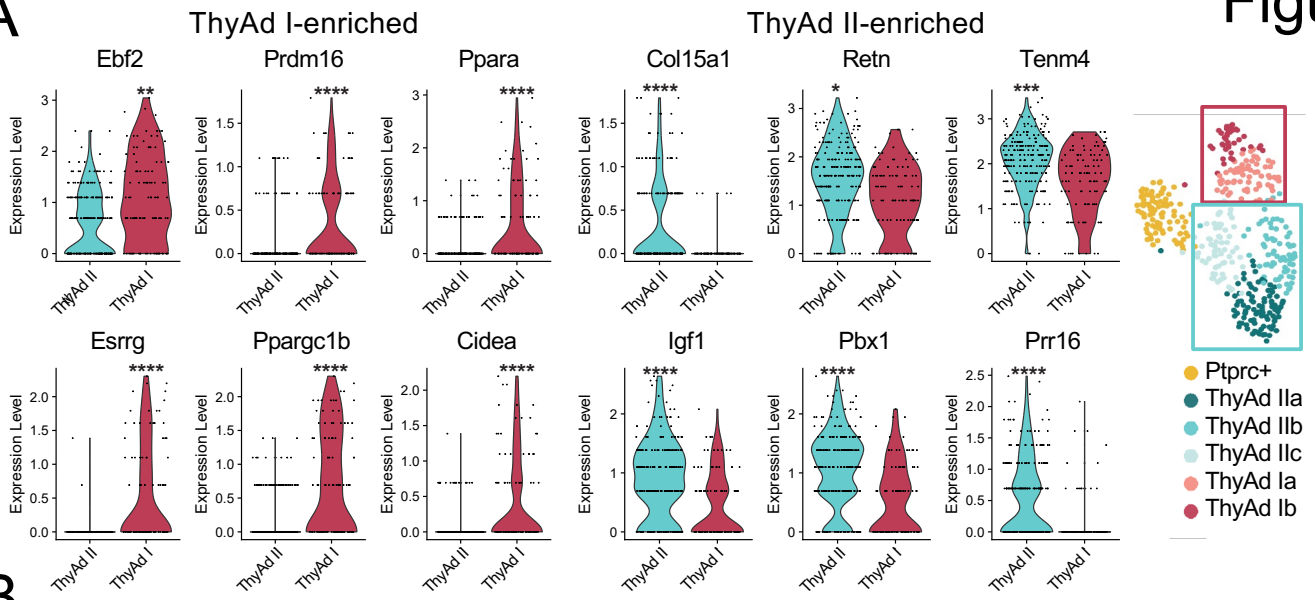

B

ThyAd I GO-Biological Process	NES	pval
Apoptotic mitochondrial changes	2.87	5.5E-04
Regulation of membrane potential	2.69	5.7E-04
Mitochondrial organization	2.39	7.8E-04
Regulation of anatomical structure morphogenesis	2.37	6.4E-04
Positive regulation of cold induced thermogenesis	2.30	4.9E-03
Sensory organ development	2.28	4.7E-03
Defense response to other organism	2.26	3.2E-03
Learning	2.26	9.5E-03
Regulation of lipid metabolic process	2.15	5.8E-03
Electron transport chain	2.12	9.6E-03
Regulation of cell projection organization	2.08	4.6E-03
ThyAd I GO-Hallmark	**NES**	**pval**
Estrogen response early	2.40	5.6E-03
Adipogenesis	2.24	4.3E-03

ThyAd II GO-Biological Process	NES	pval
Cell adhesion	2.68	1.9E-05
Extrinsic apoptotic signaling pathway	2.63	1.5E-03
Regulation of endothelial cell migration	2.61	5.0E-04
Negative regulation of developmental process	2.45	3.1E-04
Response to inorganic substance	2.30	2.2E-03
ATP synthesis coupled electron transport	2.30	5.4E-03
Regulation of locomotion	2.27	5.1E-04
Positive regulation of cellular catabolic process	2.16	9.9E-03
Regulation of cell population proliferation	2.02	3.4E-03
ThyAd II GO-Hallmark	**NES**	**pval**
Bile acid metabolism	2.26	6.6E-03
Epithelial mesenchymal transition	2.25	7.2E-03

Figure 3

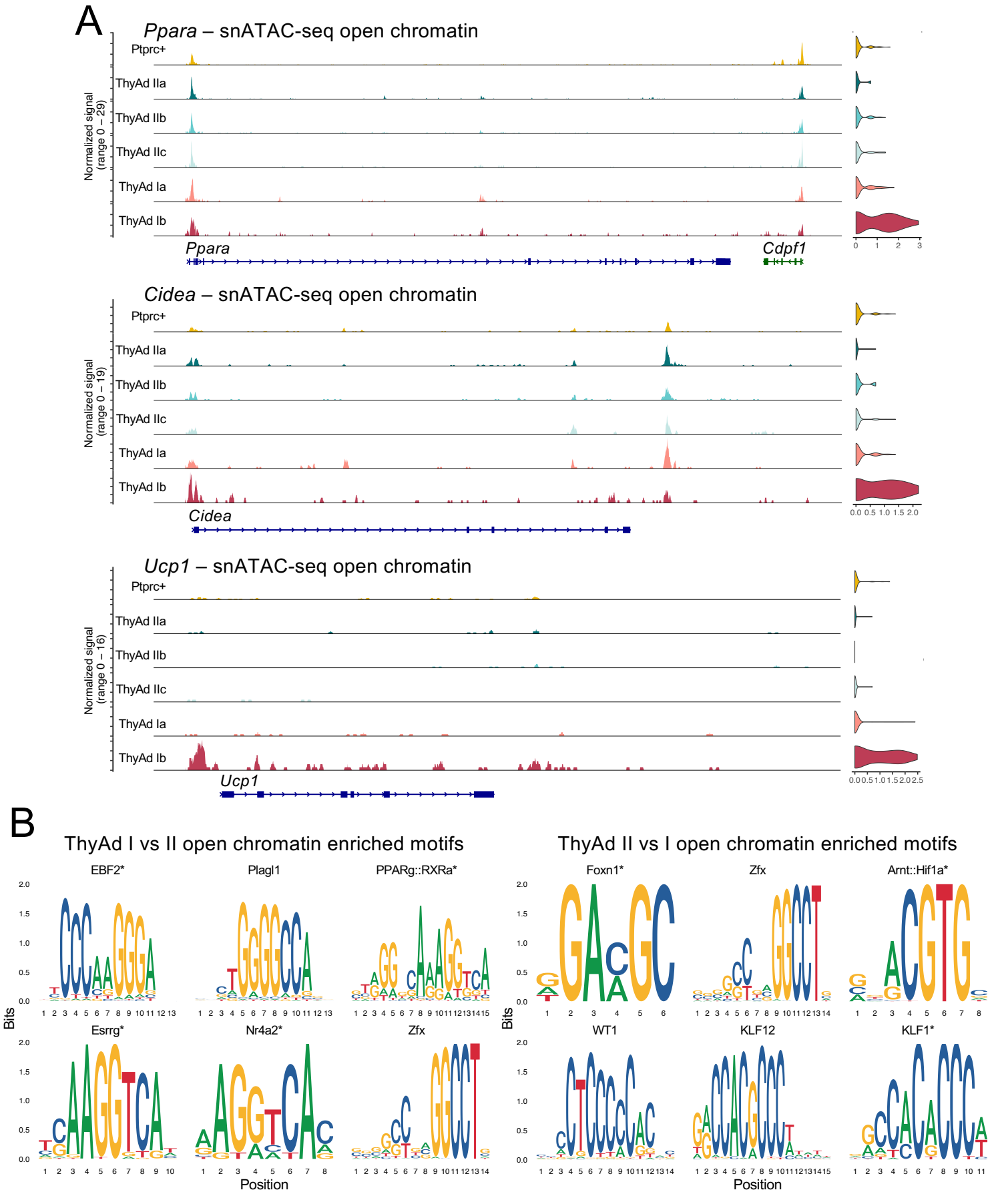
A
Ppara – snATAC-seq open chromatin
Ptprc+
ThyAd IIa
ThyAd IIb
ThyAd IIc
ThyAd Ia
ThyAd Ib
Normalized signal (range 0 – 29)
Ppara
Cdpf1
Cidea – snATAC-seq open chromatin
Normalized signal (range 0 – 19)
Cidea
Ucp1 – snATAC-seq open chromatin
Normalized signal (range 0 – 16)
Ucp1
B
ThyAd I vs II open chromatin enriched motifs
EBF2*
Plagl1
PPARg::RXRa*
Esrrg*
Nr4a2*
Zfx
ThyAd II vs I open chromatin enriched motifs
Foxn1*
Zfx
Arnt::Hif1a*
WT1
KLF12
KLF1*
Bits
Position

Figure 4

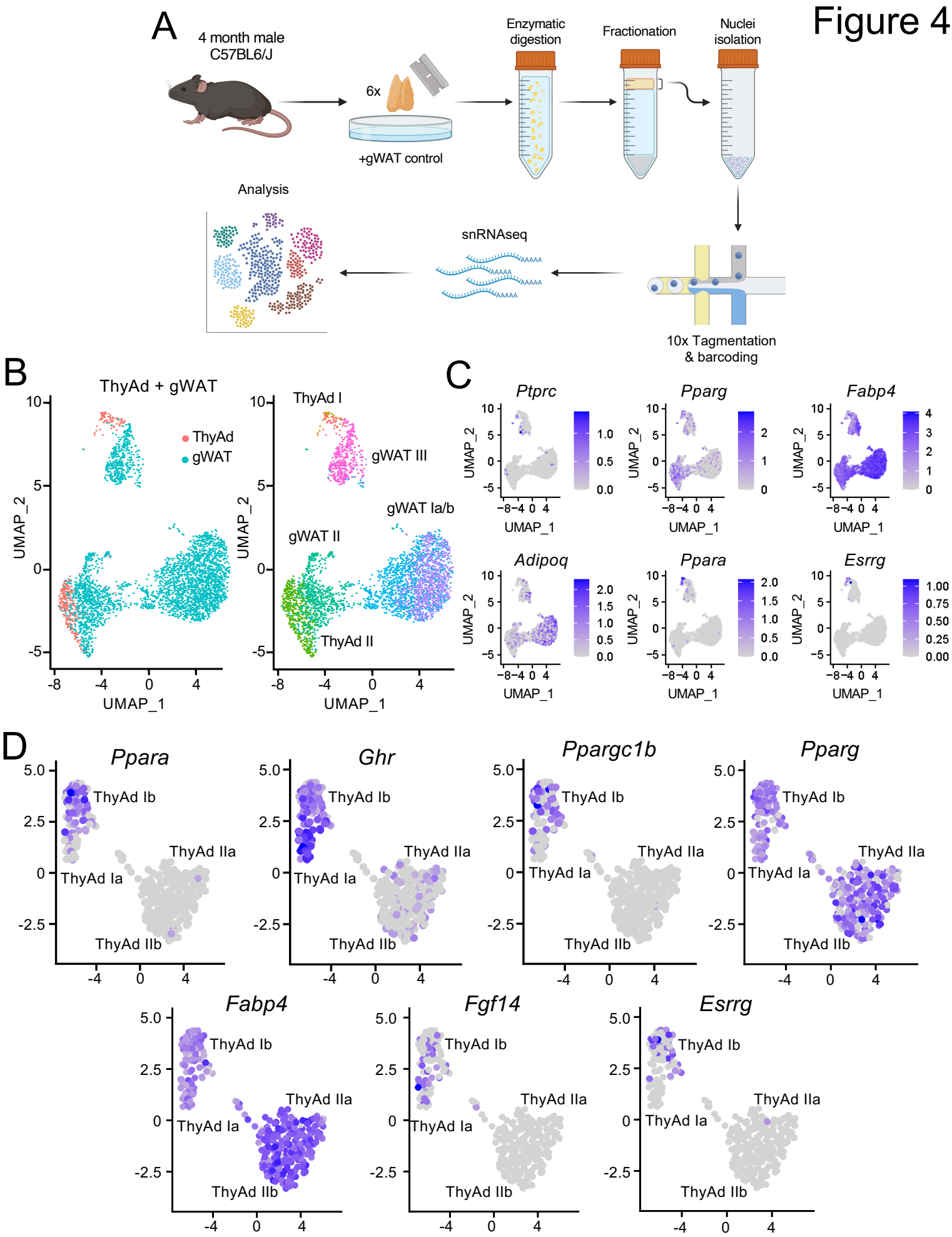
A
4 month male
C57BL6/J
6x
+gWAT control
Enzymatic
digestion
Fractionation
Nuclei
isolation
10x Tagmentation
& barcoding
snRNAseq
Analysis
B
ThyAd + gWAT
ThyAd
gWAT
ThyAd I
gWAT III
gWAT Ia/b
gWAT II
ThyAd II
UMAP_1
UMAP_2
C
Ptprc
Pparg
Fabp4
Adipoq
Ppara
Esrrg
D
Ppara
Ghr
Ppargc1b
Pparg
Fabp4
Fgf14
Esrrg
ThyAd Ib
ThyAd Ia
ThyAd IIa
ThyAd IIb

Figure 5

A

Minus 1° antibody

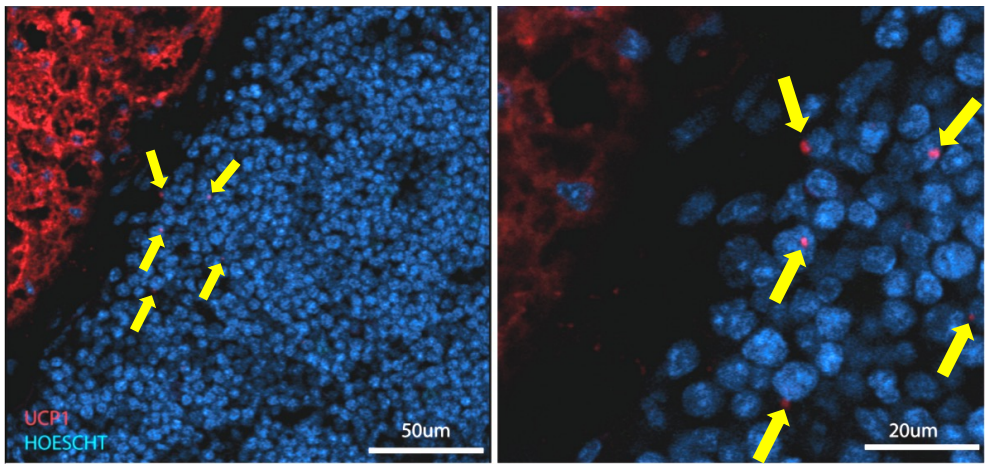

Adjacent section With 1° antibody

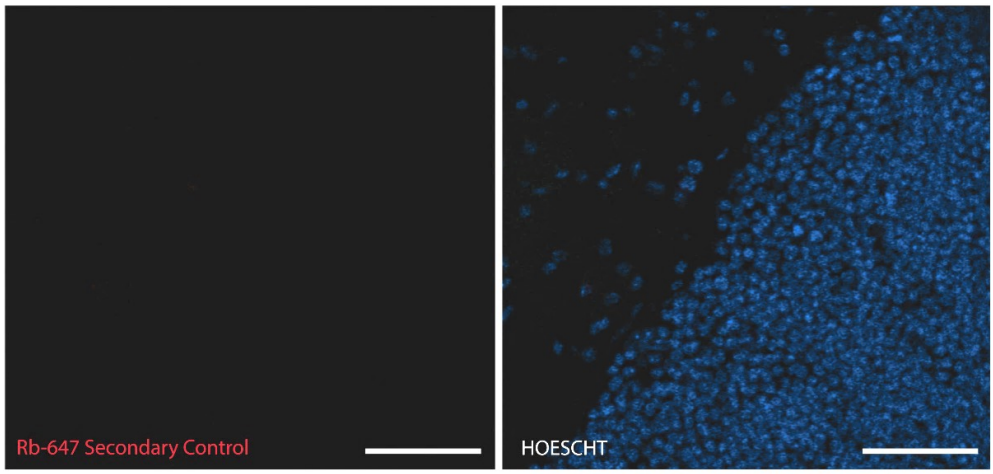

B

Minus 1° antibody

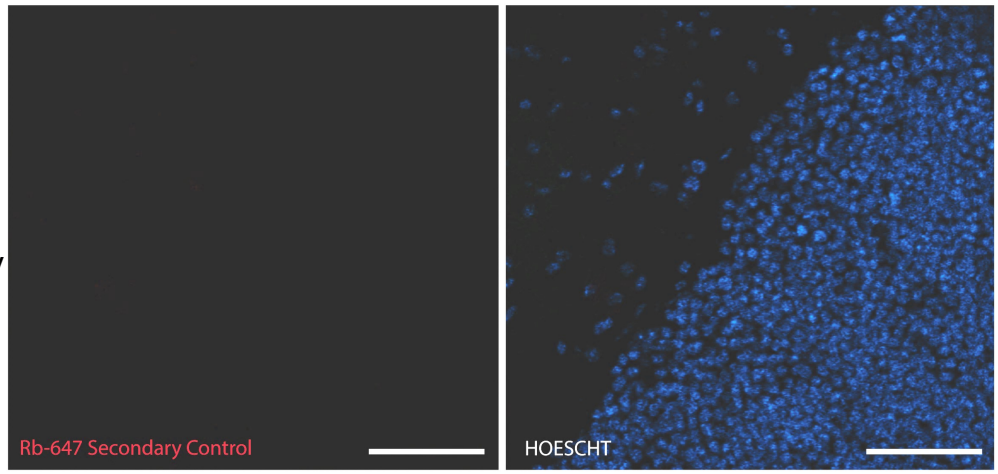
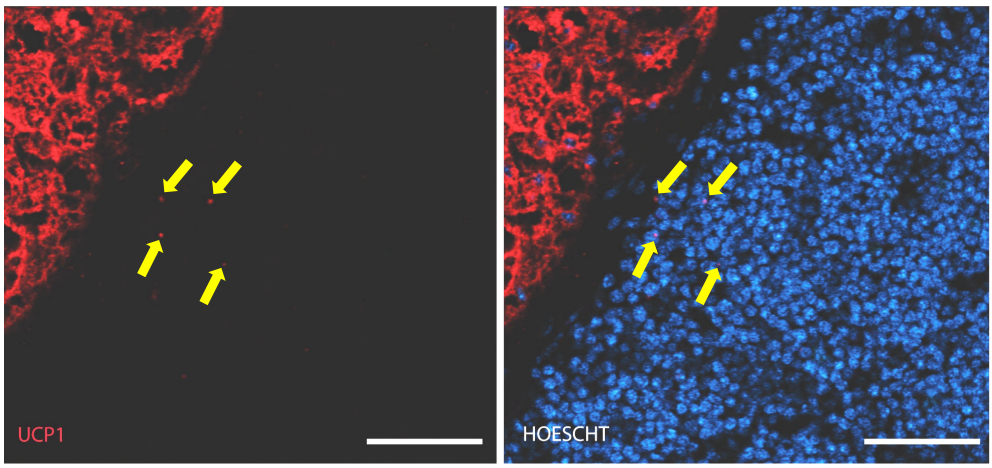
Adjacent section With 1° antibody